Compositional Dependent Thin Film Stress States

G. B. Thompson – The University of Alabama
B. Fu – The University of Alabama

Citation of published version:

Thompson, G., Fu, B. (2010): Compositional Dependent Thin Film Stress States. *Journal of Applied Physics*, 108(4). DOI: https://doi.org/10.1063/1.3462431

Compositional dependent thin film stress states

B. Fu and G. B. Thompson[a)]
Department of Metallurgical and Materials Engineering, The University of Alabama, Tuscaloosa, Alabama 35487-0202, USA

(Received 8 January 2010; accepted 9 June 2010; published online 18 August 2010; publisher error corrected 23 August 2010)

This paper addresses *in situ* stress evolution of two-component Fe_xPt_{1-x}, where x spanned 0 to 1, alloy thin films. The stresses of the high-temperature, quenched-in, solid solution phase was determined by *in situ* wafer curvature measurements during ambient temperature growth. The measured stresses were shown to be compositional dependent and spanned both compressive and tensile stress states. Under specific growth conditions, a "zero-stress" state could be achieved. The alloy stress states did not show any significant stress recovery upon ceasing the deposition, i.e. the stress state during growth was retained in the film. X-ray diffraction, transmission electron microscopy, and atom probe tomography were used to characterize the microstructures of each thin film. The evolution of the stress state with composition is described in terms of a chemical potential term for preferential segregation of one species in the alloy to the grain boundaries. © *2010 American Institute of Physics*. [doi:10.1063/1.3462431]

I. INTRODUCTION

Thin films prepared by physical vapor deposition can undergo large intrinsic stresses which can be higher than their bulk phase modulus. This intrinsic stress plays an important role in tuning the physical[1–3] and mechanical[4] properties of the thin films and can be responsible for the failure of technologically important thin film devices.[5] By understanding stress evolution during thin film growth, and even controlling the stress state in thin films, will help improve their properties[1–6] and enhance the reliable performance of thin film based devices.

Extensive *in situ* thin film stress state studies[7–14] have been performed during the deposition of various single elemental films. It has been revealed that high adatom mobility films like Cu [10,12] and Ag [7–10] usually undergo compressive-to-tensile-to-compressive stress evolution corresponding to the nucleation of islands, coalescence of islands, and post-growth stages. In contrast, low adatom mobility films such as Fe,[11,14] Cr,[11] and Co,[13] only experience compressive-to-tensile changes.

Thin film growth stress is very sensitive to experimental parameters, such as deposition temperature,[11,14] deposition rate,[9,15] and pressure.[12,13] Based on experiments and simulations,[9,14,16–19] various theoretical models[9,14,16–19] have been proposed to explain and even predict the stress evolution during thin film growth. It is generally accepted that the initial compression is a result of the early-stage embryonic/island formation of the atoms converging to minimize surface area to volume energies. The tensile stress originates from the strain associated with the coalescence of these islands to minimize the grain boundary energy. The mechanism of postcoalescence compressive stress is still under discussion.[9,14,18,19] It is thought to originate from either extra atoms being inserted into the grain boundaries[9,18] or a locked-in capillarity stress[19] or because of grain growth and recrsytallization.[14]

While most of experimental research about *in situ* stress has been focused on single metallic elements, there is less information about metallic alloy systems.[20,21] Alloys can result in co-operative adatom mobility and free surface and grain boundary segregation for different species which will result in different growth stresses. Similar to mixed compounds,[22,23] controlling the alloy chemistries could be used to tune the growth stresses. In this paper, the as-deposited *in situ* stress measurements of the binary alloy Fe_xPt_{1-x}, where x spanned 0 to 1, was used to investigate the influences and mechanisms of composition dependent growth stresses in thin films.

II. EXPERIMENTAL DETAILS

The Fe_xPt_{1-x} alloy thin films were cosputter-deposited from >99.5% pure elemental targets to a thickness of 40 nm onto Si [001] substrates, with native surface oxide, in an AJA ATC-1500 stainless-steel chamber at ambient temperature (~25 °C). As previously mentioned, pressure[12,13] and temperature[11,14] can influence the final stress state and is the subject of future work. The base pressure prior deposition was $<1\times10^{7}$ Torr where upon ultrahigh purity Ar was flowed at 10 standard cubic centimeters per minute to 2 mTorr for sputtering and served as the sputtering working gas. The k-Space Associates' multibeam optical sensor system (MOSS) was used to measure the *in situ* stress state during deposition. The MOSS measures the change in the radius of the curvature of the substrate from a reflected laser beam passed through an echelon and collected on a charge coupled device camera.[24] The displacement of the reflected laser spots is then used to calculate the average stress according to Stoney's equation,[25]

a)Electronic mail: gthompson@eng.ua.edu.

$$\sigma = -\frac{1}{12}\frac{E_s}{1-v_s}\frac{\cos(\alpha)t_s^2}{Lt_f}\left(\frac{1}{R_1}-\frac{1}{R_0}\right), \quad (1)$$

where $E_s/(1-v_s)$ is the biaxial modulus of the substrate, t_s and t_f are the thickness of the substrate and thin film, α is the angle of incidence of the laser beam, L is the substrate-detector optical length, and R_0 and R_1 are the radius of curvature of the measured substrate before and during/after film deposition. The values of these parameters are the following: the biaxial modulus of the substrate was taken as 180 GPa,[26] thickness of the Si [100] substrate was ~250 μm, L was 88 cm, and α was 2°. The growth rates were determined from the final film thickness divided by the time of deposition and were controlled by the sputtering power. The thicknesses were verified by small angle x-ray reflectivity[27] using an X'Pert Philips x-ray diffractometer operated with a Cu K_α source at 45 kV and 40 mA.

The average compositions of the alloy thin films was determined by the individual growth rates from each target and verified using scanning electron microscopy (SEM)-energy dispersion spectrometry on a Philips XL30 operated at 30 kV. X-ray diffraction (XRD) was performed for phase identification using a Philips APD diffractometer with a Cu K_α radiation source operated at 40 kV and 35 mA. The average grain size was calculated from transmission electron microscopy (TEM) bright/dark field imaging using a Tecnai F20 (scanning) TEM. At least 100 grains were averaged and the standard error was calculated. The selected area electron diffraction (SAED) patterns were also taken to identify the phases of the alloy thin films.

Atom probe samples were prepared by *in situ* lift-out of a wedge from the thin film wafer, in a similar manner reported by Thompson *et al.*[28] and modified for thin films by Torres and Thompson.[29] The samples were focus ion milled using a FEI Quanta 3D dual-beam focus ion beam-SEM. The annular mill to shape the film into the required atom probe tip geometry used an ion beam current between 0.3–1.0 nA at 30 KeV. A final 5 KeV "clean up" step was used to reduce the Ga implantation damage to the surface of the sample. The atom probe tips were analyzed in an Imago Scientific Instruments Local Electrode Atom Probe (LEAP®) 3000XSi in a laser pulsing mode. The field evaporation events were run at a base temperature of 50 K with laser pulse energy of 0.3–0.5 nJ at a pulse rate of 250 kHz. Lower base temperatures and lower pulse energies resulted in a propensity of tip fracture failures during field evaporation.

III. RESULTS

The *in situ* stress evolution of the 40 nm thick Fe, $Fe_{0.82}Pt_{0.18}$, $Fe_{0.65}Pt_{0.35}$, $Fe_{0.54}Pt_{0.46}$, $Fe_{0.45}Pt_{0.55}$, $Fe_{0.28}Pt_{0.72}$, $Fe_{0.21}Pt_{0.79}$, and Pt thin films are displayed in Fig. 1(a). From Fig. 1(a), the Fe thin film experiences a compressive-to-tensile stress transition and the Pt thin film exhibits a compressive-to-tensile-to-compressive stress transition, which is consistent with similar reports in the literature.[5,11,14] The Fe–Pt alloy films formed a solid solution, as will be discussed and shown in the XRD and electron diffraction figures below. It is found that the $Fe_{0.65}Pt_{0.35}$ thin film showed a residual stress near zero at 40 nm thickness. The residual stress is the stress state value at the end of the deposition at a fixed thickness. Also, it is interesting to note that for alloy films >35 at. % Pt, the stress state no longer obeyed a linear mixing trend, Fig. 1(b).

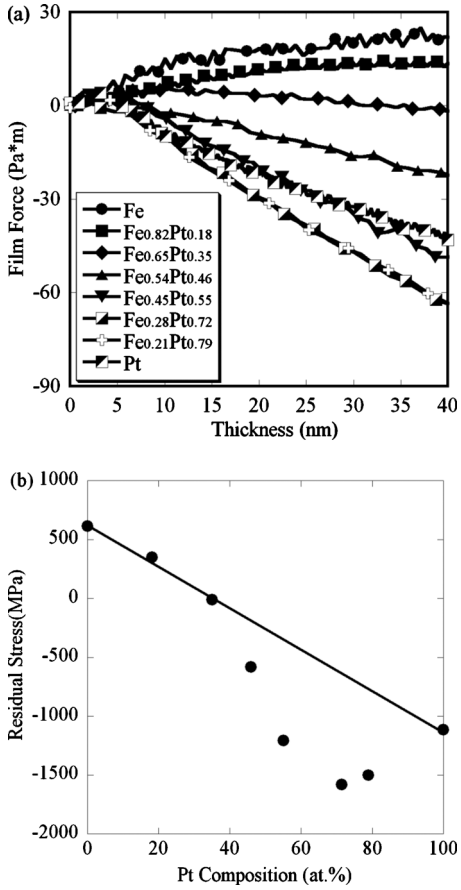

FIG. 1. (a) Growth stresses of the Fe–Pt thin film system (b) Residual intrinsic stresses measured at the end of the depositions of a 40 nm film. The deposition rates for the Fe, $Fe_{0.82}Pt_{0.18}$, $Fe_{0.65}Pt_{0.35}$, $Fe_{0.54}Pt_{0.46}$, $Fe_{0.45}Pt_{0.55}$, $Fe_{0.28}Pt_{0.72}$, $Fe_{0.21}Pt_{0.79}$, and Pt thin films are 0.1 nm/s, 0.11 nm/s, 0.15 nm/s, 0.18 nm/s, 0.2 nm/s, 0.3 nm/s, 0.4 nm/s, and 0.05 nm/s, respectively. Note that the residual stress varies as a function of composition.

Since deposition rates can affect the mobility of adatoms hence the stress state, the "zero-stress" $Fe_{0.65}Pt_{0.35}$ and "compressive stress" $Fe_{0.45}Pt_{0.55}$ thin film was deposited at different deposition rates. Unlike single element films, which can exhibit significant changes in stress with deposition rate,[9,15] the growth stress for these alloys showed very little change with the deposition rates studied, as seen in Fig. 2. Changing the rates to span a larger range, at a fixed thickness and composition, proved experimentally difficult using two separate elemental sputtering sources. Each source has its own intrinsic rate of growth with sputtering power. For such studies, fixed alloyed targets would be more amenable in consistently controlling the rate for a fixed composition, particularly at extremes in low or high deposition rates and should be considered for future studies.

The XRD results of the as-deposited thin films for the eight different compositions is plotted in Fig. 3(a). Each film is highly textured with the closest packed planes being parallel to the growth direction. The elemental Fe film was in-

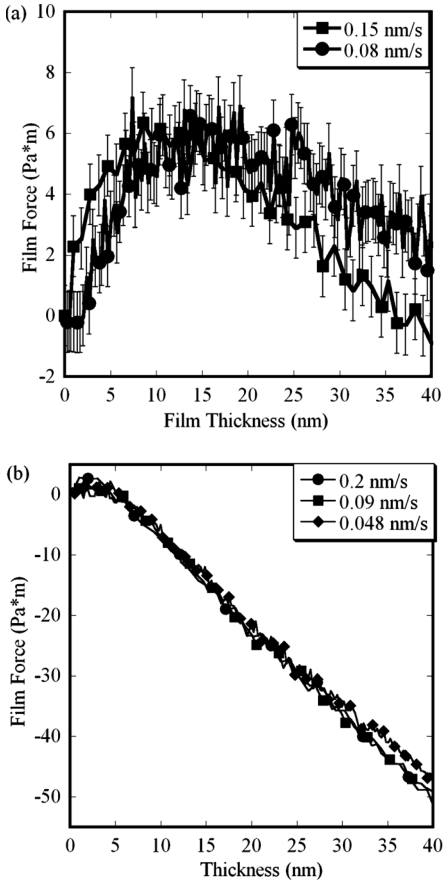

FIG. 2. Growth stresses of (a) $Fe_{0.65}Pt_{0.35}$ and (b) $Fe_{0.45}Pt_{0.55}$ thin films grown at different deposition rates. The error bar in (b) is smaller than the Markers because of the Y-scale.

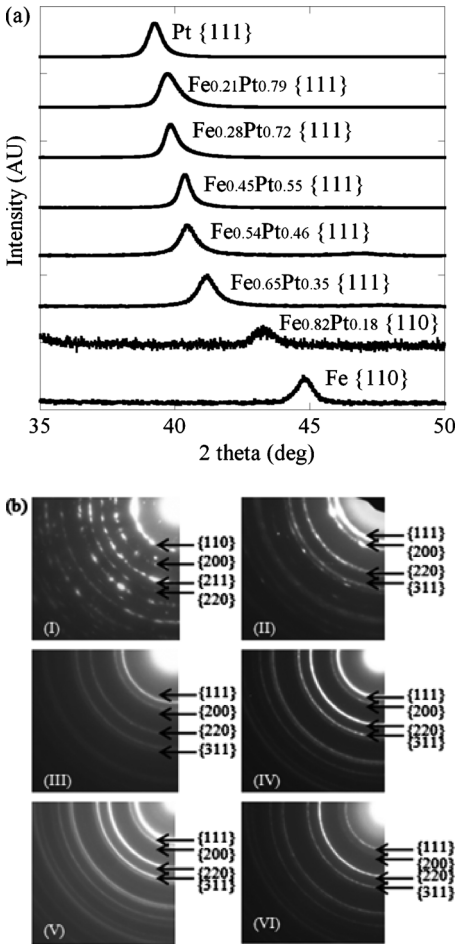

FIG. 3. (a) XRD spectra for the Fe, $Fe_{0.82}Pt_{0.18}$, $Fe_{0.65}Pt_{0.35}$, $Fe_{0.54}Pt_{0.46}$, $Fe_{0.45}Pt_{0.55}$, $Fe_{0.28}Pt_{0.72}$, $Fe_{0.21}Pt_{0.79}$, and Pt thin films using Cu $K\alpha$ x-rays; (b) SAED pattern of the (I) $Fe_{0.82}Pt_{0.18}$, (II) $Fe_{0.65}Pt_{0.35}$, (III) $Fe_{0.54}Pt_{0.46}$, (IV) $Fe_{0.45}Pt_{0.55}$, (V) $Fe_{0.28}Pt_{0.72}$, and (VI) $Fe_{0.21}Pt_{0.79}$ thin film. The diffraction pattern indexes $Fe_{0.82}Pt_{0.18}$ thin film to a bcc symmetry while the other alloy thin films to fcc symmetry.

dexed as body centered cubic (bcc) where as the elemental Pt was face centered cubic (fcc). The $Fe_{0.82}Pt_{0.18}$ thin film adopted a solid solution bcc phase and all other alloy composition adopted a solid solution fcc phase. This fcc phase is consistent with the literature[30] and is the quenched-in high-temperature phase for this system. The in-plane grain size of these thin films, Fig. 4, were very similar with values that ranged from ~8 to 16 nm.

The atom probe results are shown in Fig. 5. For the elemental Pt thin film, very distinct grain boundaries can be seen in the reconstructed atom map of Fig. 5(a). The reconstruction of these boundaries are a result of trajectory aberrations because of the density variation in the boundaries.[31–33] The grain sizes in the atom map are in reasonable agreement with the previous size measurements from TEM plotted in Fig. 4. The reconstructed Pt atom map for the $Fe_{0.54}Pt_{0.46}$ thin films showed clear grain boundaries. Previous TEM Frensel contrast imaging of a thin film atom probe tip of a similar composition has confirmed that these reconstruction variations are consistent with the shape and size of the deposited grains.[29] This grain boundary reconstruction would be a result of either a density and/or compositional variation within the boundary.[31–33] Again, the grain size in these atom maps, Fig. 5(c), are consistent with those measured using TEM images given in Fig. 4. The one-dimensional (1D) compositional profile of a grain boundary in the $Fe_{0.54}Pt_{0.46}$ film, Fig. 5(d), showed an enrichment of Pt in the boundary, which is consistent with literature predictions that Pt would preferentially be on the surface of nanoscale FePt.[29,34,35] However, for the $Fe_{0.65}Pt_{0.35}$ thin film, it was difficult to distinguish the grain boundaries from the atom map reconstructions. The 1D compositional profile for

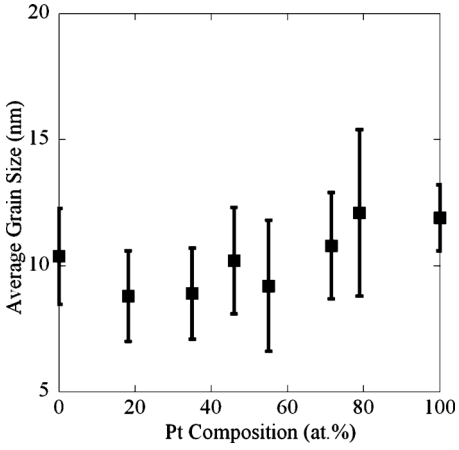

FIG. 4. The average grain size of those thin films measured from TEM bright/dark field images.

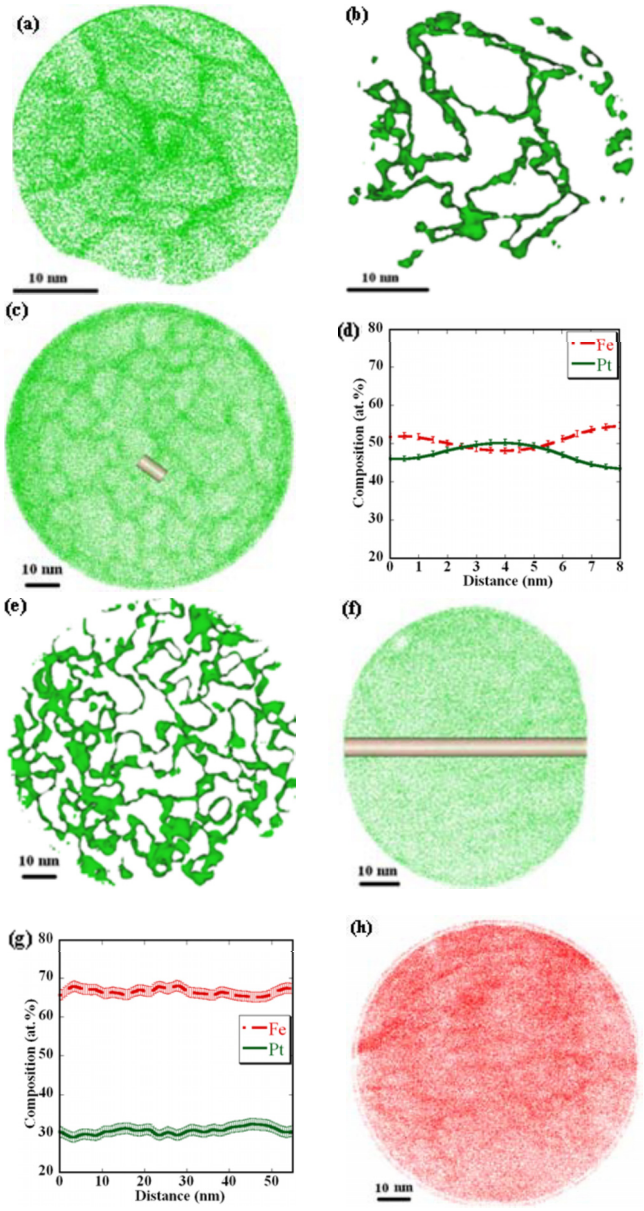

FIG. 5. (Color online) (a) Pt atom map in the pure Pt film. (b) Pt iso-density surface which closely maps the density variations (grain boundaries) in (a). (c) Pt atom map in the $Fe_{0.54}Pt_{0.46}$ film. (d) 1D compositional profile from (c). (e) Iso-concentration surface created at 47.2 at. % Pt, which is higher than the average Pt content. The iso-density surface closely maps the density variations (grain boundaries) in (c). (f) Pt atom map in the $Fe_{0.65}Pt_{0.35}$ film. (g) 1D compositional profile from (f). (h) Fe atom map for the Fe film.

$Fe_{0.65}Pt_{0.35}$ goes across the entire atom map and does not show any significant variations in composition. Based on the grain size of this film and the field of view of the atom map, the profile would intersect several grain boundaries. The elemental Fe thin film does not show distinct grain boundaries in the atom map of Fig. 5(h).

IV. DISCUSSION

The *in situ* stress measurements for the Fe_xPt_{1-x} alloy thin films are strongly dependent on their compositions. There has been considerable discussion in the literature on the origins of thin film stress states. Chason *et al.*[9] have proposed that the compressive stress during postcoalescence is caused by the adatoms reversibly moving in and out of the grain boundaries. The driving force for those extra atoms to the grain boundaries is from the increase in the surface chemical potential during deposition because of the arrival and flow of deposited atoms on the surface.[9] For alloy films with a composition >35 at. % Pt, the stress deviated from a linear mixing trend. This deviation is interpreted in terms of Chason *et al.*'s model.[9]

The chemical potential difference between the surface and grain boundaries for a binary alloy system can be rewritten as[9]

$$\Delta\mu' = \mu_s - \mu_{gb} = \Delta\mu_0 + \delta\mu_s + \sigma\Omega - \mu_c, \tag{2}$$

where $\Delta\mu_0$ is the difference between the surface and grain boundary chemical potential in absence of growth (usually small and negligible), $\delta\mu_s$ is the increase in surface chemical potential because of the flux of deposited atoms, σ is the stress along the grain boundary, Ω is the atomic volume, and μ_c is chemical potential rise in the grain boundary because of the aggregation of extra, high adatom mobility atoms. We have added the latter term, μ_c, to describe the chemical potential driving force of preferential segregation of one species to another to the boundaries. This last term is consistent with the emergent chemical potential driving forces observed in other thermochemical systems. For instance, simulation studies have clearly identified chemical potential driving forces for composition enrichment and equilibrium shifts at vapor-liquid interfaces.[36] In fact, these modeling studies have predicted that modifications to the interfacial stress can actually be used to tune the composition at a vapor-liquid interface.[37] The underlying physics of this driving force can be separated into entropic and enthalpic contributions. Given the fact that compositional enrichment (demixing) likely decreases the local entropy, the primary driving force for the enrichment should be attributed to enthalpy minimization.

For a binary alloy, differences in intrinsic mobility between each species can induce preferential segregation of the higher mobile species to the grain boundaries. This grain boundary segregation yielded an additional chemical potential. For highly mobile films, like Pt, the addition of Fe changes the grain boundary chemical potential and can reduce the force that is driving atoms toward the grain boundaries. Alternatively, the low mobility films, like Fe, can have their grain boundary chemical potential facilitate the mobility of atoms to the boundary by the addition of Pt. The atom probe tomography grain boundary analysis of $Fe_{0.54}Pt_{0.46}$ thin films indicated a preferential segregation of Pt above the bulk Pt film composition at the boundaries, even for an overall Fe-rich film, and is consistent with previous studies.[29] This result supports the notion that higher mobility atoms can segregate to the grain boundaries and contribute to the compositional dependent stress behavior. The segregation of the higher mobility atoms to the grain boundaries, even in films with overall enriched low mobility atom compositions, can contribute to controlling the stress state as a function of composition and to the deviation of stress states from linear mixing. Thus, the μ_c can be decreased with increasing composition of the higher mobile species, Pt, and the films can become more compressive according to the modified addi-

tion to Chason *et al.*'s model.[9] It is also interesting to note that at a very high Pt composition (for the $Fe_{0.28}Pt_{0.72}$ and $Fe_{0.21}Pt_{0.79}$ thin films), this negative deviation from linear mixing behavior is decreased with increasing Pt content. Since the Pt atoms are larger than Fe atoms, the density difference between the grain boundaries and the grains would be less with increasing overall Pt content. The effect of the segregation of Pt atoms to the grain boundaries to generate extra compressive stress would become less for very high Pt content thin films and could explain the recovery back toward the linear mixing observation for the Pt film, Fig. 1(b).

The deviations from linearity observed in Fig. 1(b) appeared to be consistent with the deviations observed in simple model systems of interfacial stresses.[36] For instance, as the particle-particle energy is methodically changed in the molecular modeling studies, there is a nonlinear transition observed in the interfacial stress.[36] However, as the particle sizes are methodically increased, the shift in the interfacial stress appeared to be more linear[36] and this particle size effect is most likely associated with an entropic phenomena. The primary driving force for the chemical enrichment at the grain boundaries is likely because of the enthalpy minimization contribution to the chemical potential driving force and this is consistent with the shape of the curve in Fig. 1(b).

A cross-over point of zero-stress can be achieved between the tensile and compressive states of the film. This provides a means to tune in a desired stress within a film. This "zero-state" represents a balance between the adatoms moving to the boundaries and those growing vertically off the surface. As mentioned previously, trajectory aberrations in the atom maps that reveal grain boundaries are a result of compositional fluctuations, density variations and/or surface modifications.[31–33] The visual appearances in the $Fe_{0.54}Pt_{0.46}$ and Pt atom maps for these grain boundaries are a result of these variations. This provides experimental evidence that these films, which are in compression, are a result of an increase in the atomic density in the boundaries.

For the zero-stress $Fe_{0.65}Pt_{0.35}$ film, the atom map showed little to no trajectory aberrations, indicative of little to no compositional, density or surface variations across the boundaries. The compositional profile that spanned the entire atom map would, on average, intersect approximately five grains or ten grain boundaries (one on each side) based on the TEM determined grain sizes and field of view of the atom map. The composition profile, Fig. 5(g), showed no significant compositional variation. This would suggest no compositional segregation existed in the boundary and the two species, Fe (tensile) and Pt (compressive) are balanced.

The stress recovery after deposition for the Fe_xPt_{1-x} systems is depicted on Fig. 6. The stress behavior in the Fe_xPt_{1-x} system did not reveal a significant change (or recovery) upon ceasing the growth of the film. It has been noted in other systems, like Ag,[7–10] the compressive stress can relax upon stopping the growth of the film. Chason *et al.*[9] has described this recovery in terms of a change in the surface chemical potential, $\delta\mu_s$, described previously. The lack of a stress change upon ceasing the growth suggests that (1) the surface chemical potential between a condition of deposition and nondeposition is minor, (2) these atoms do not have sufficient thermal mobility in the as-deposited condition for recovery, and/or (3) the lack of a sufficient compressive state condition for the atoms to migrate out of the boundaries. Koch *et al.*[14] have reported a recovery of elemental Fe's stress state at elevated temperatures suggesting Fe has limited mobility at room temperature. The preservation of a stress state for these alloyed films, even after deposition, provided the ability to retain the stress condition and potentially tune these films' mechanical behavior and failure modes at room temperature.

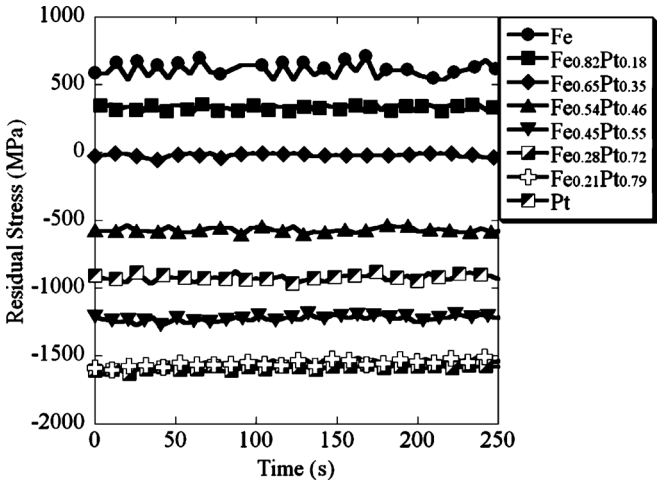

FIG. 6. The evolution of the average intrinsic stress after the deposition of the thin films with a final thickness of 40 nm.

V. CONCLUSIONS

A series of 40 nm Fe_xPt_{1-x} thin films have been magnetron sputter-deposited onto Si [001] substrates. The *in situ* stress evolution of elemental Fe and Pt and their range of solid solution alloys has been measured. It was found that the intrinsic stress state could be tuned to be either tensile, zero or compressive depending upon composition for similar grain sizes. The Pt element was found to be the more mobile atom as compared to Fe. The films near a zero-stress state had little to no compositional segregation of one species enriching the boundaries as compared to the bulk of the grains. We have provided a modified version of Chason *et al.*'s[9] thin film growth model to include a chemical potential term for the preferential segregation of one species to the grain boundaries. The enrichment of one species at the grain boundaries controlled the stress state toward the intrinsic elemental stress condition, i.e., compressive or tensile. This has been used to describe how the stress state can be varied in a multicomponent system. Finally, these intrinsic stress states of the alloy films studied appeared to be retained, even upon ceasing deposition at ambient temperature.

ACKNOWLEDGMENTS

The authors gratefully recognize the National Science Foundation (Grant No. DMR-0529369) and the Alabama Commission on Higher Education Graduate Research Scholars Program for supporting this research. The Tecnai TEM

and LEAP 3000XSi were acquired through the National Science Foundation Major Instrumentation Program (Grant No. DMR–0421376 and DMR-0722631, respectively).

[1]J. Barbosa, B. Almeida, A. M. Pereira, J. P. Araújo, I. Gomes, and J. Mendes, J. Non-Cryst. Solids **354**, 5250 (2008).
[2]A. Miyamura, K. Kaneda, Y. Sato, and Y. Shigesato, Thin Solid Films **516**, 4603 (2008).
[3]J. Zhu, Y. R. Li, Y. Zhang, X. Z. Liu, and B. W. Tao, Ceram. Int. **34**, 967 (2008).
[4]C. T. Chuang, C. K. Chao, R. C. Chang, and K. Y. Chu, J. Mater. Process. Technol. **201**, 770 (2008).
[5]R. Koch, J. Phys.: Condens. Matter **6**, 9519 (1994).
[6]G. C. A. M. Janssen, Thin Solid Films **515**, 6654 (2007).
[7]R. Koch, D. Winau, A. Führmann, and K. H. Rieder, Phys. Rev. B **44**, 3369 (1991).
[8]R. Abermann and R. Koch, Thin Solid Films **129**, 71 (1985).
[9]E. Chason, B. W. Sheldon, L. B. Freund, J. A. Floro, and S. J. Hearne, Phys. Rev. Lett. **88**, 156103 (2002).
[10]D. Winau, R. Koch, A. Führmann, and K. H. Rieder, J. Appl. Phys. **70**, 3081 (1991).
[11]G. Thurner and R. Abermann, Thin Solid Films **192**, 277 (1990).
[12]M. Pletea, W. Bruckner, H. Wendrock, and R. Kaltofen, J. Appl. Phys. **97**, 054908 (2005).
[13]M. Pletea, W. Bruckner, H. Wendrock, R. Kaltofen, and R. Koch, J. Appl. Phys. **99**, 033509 (2006).
[14]R. Koch, D. Hu, and A. K. Das, Phys. Rev. Lett. **94**, 146101 (2005).
[15]A. L. Del Vecchio and F. Spaepen, J. Appl. Phys. **101**, 063518 (2007).
[16]R. C. Cammarata, T. M. Trimble, and D. J. Srolovitz, J. Mater. Res. **15**, 2468 (2000).
[17]W. D. Nix and B. M. Clemens, J. Mater. Res. **14**, 3467 (1999).
[18]C. W. Pao, S. M. Foiles, E. B. Webb, D. J. Srolovitz, and J. A. Floro, Phys. Rev. Lett. **99**, 036102 (2007).
[19]C. Friesen, S. C. Seel, and C. V. Thompson, J. Appl. Phys. **95**, 1011 (2004).
[20]St. Bertel and R. Abermann, Thin Solid Films **473**, 1 (2005).
[21]M. Pletea, H. Wendroch, R. Kaltofen, O. G. Schmidt, and R. Koch, J. Phys.: Condens. Matter **20**, 255215 (2008).
[22]H. Sankur, W. J. Gunning, and J. F. DeNatale, Appl. Opt. **27**, 1564 (1988).
[23]H. O. Sankur, J. DeNatale, and W. J. Gunning, Appl. Opt. **30**, 495 (1991).
[24]C. Taylor, D. Bartlett, E. Chason, and J. Floro, The Industrial Physicists **4**, 25 (1998).
[25]G. G. Stoney, Proc. R. Soc. London, Ser. A **82**, 172 (1909).
[26]K. E. Peterson, Proc. IEEE **70**, 420 (1982).
[27]Y. Sasanuma, M. Uchida, K. Okada, K. Yamamoto, Y. Kitano, and A. Ishitani, Thin Solid Films **203**, 113 (1991).
[28]K. Thompson, D. Lawrence, D. J. Larson, J. D. Olson, T. F. Kelly, and B. Gorman, Ultramicroscopy **107**, 131 (2007).
[29]K. L. Torres and G. B. Thompson, Ultramicroscopy **109**, 606 (2009).
[30]C. M. Kuo, P. C. Kuo, and H. C. Wu, J. Appl. Phys. **85**, 2264 (1999).
[31]M. K. Miller, A. Cerezo, M. G. Hetherington, and G. D. W. Smith, *Atom Probe Field Ion Microscopy* (Clarendon, Oxford, 1996), p. 196.
[32]M. K. Miller and M. G. Hetherington, Surf. Sci. **246**, 442 (1991).
[33]M. Thuvander and H.-O. Andrén, Mater. Charact. **44**, 87 (2000).
[34]B. Yang, M. Asta, O. N. Mryasov, T. J. Klemmer, and R. W. Chantrell, Scr. Mater. **53**, 417 (2005).
[35]R. V. Chepulskii and W. H. Butler, Phys. Rev. B **72**, 134205 (2005).
[36]C. H. Turner, J. Phys. Chem. B **109**, 23588 (2005).
[37]C. H. Turner, Langmuir **23**, 2525 (2007).